Articles

Effect of Hfq on RprA−*rpoS* mRNA Pairing: Hfq−RNA Binding and the Influence of the 5′ *rpoS* mRNA Leader Region†

Taylor Updegrove,‡ Nabil Wilf,‡ Xueguang Sun, and Roger M. Wartell*

School of Biology and Institute of Bioengineering and Biosciences, Georgia Institute of Technology, Atlanta, Georgia 30332

Received March 20, 2008; Revised Manuscript Received July 4, 2008

ABSTRACT: The *rpoS* mRNA encodes a stress response transcription factor in *Escherichia coli*. It is one of a growing number of mRNAs found to be regulated by small RNAs (sRNA). Translation initiation of *rpoS* mRNA is enhanced by two sRNAs, DsrA and RprA, that pair to the same site near the *rpoS* start codon in the presence of the Hfq protein. In this work, we examine the interaction of *E. coli* Hfq with RprA and two portions of the *rpoS* mRNA leader region. One *rpoS* RNA, rpoS-L, contained the entire 565-nucleotide leader region, while the other, rpoS-S, contained the 199-nucleotide sequence surrounding the start codon. An RNase H assay indicated both *rpoS* RNAs have similar secondary structures in the translation initiation region. Hfq formed two complexes with RprA in a gel mobility assay with binding parameters similar to values previously determined for DsrA. Unlike DsrA, Hfq binding to RprA was inhibited by poly(A) and influenced by Hfq mutations on both the distal and proximal surfaces. Hfq increased the level of RprA binding to both *rpoS* RNAs but showed a much larger enhancement when rpoS-L, the entire leader region, was examined. The lower affinity of RprA for rpoS-L versus rpoS-S in the absence of Hfq suggests that Hfq overcomes an inhibitory structure within rpoS-L in stimulating RprA binding. Similar results were obtained with DsrA. The results indicate that the full upstream leader sequence of *rpoS* mRNA influences Hfq-facilitated annealing of RprA and DsrA and is likely to be involved in its regulation.

Short noncoding RNAs (sRNA),[1] approximately 100 nucleotides long, have been shown to be involved in post-transcriptional regulation of mRNA expression in *Escherichia coli* and other bacteria (*1*−*4*). Characterization of a number of sRNAs indicates that many are induced under stress conditions and act in trans by base pairing to target sites on specific mRNAs, inhibiting or enhancing translation initiation. A characteristic common to this class of sRNA is their strong binding affinity for Hfq (*5*), a protein with RNA chaperone activity (*6*). Hfq was initially identified as a host factor for the replication of the RNA phage Qβ (*7*), but its importance to cell metabolism in *E. coli* was demonstrated by the widespread pleiotropic effects caused by null mutants of the *hfq* gene (*8*). Phylogenetic and structure analyses showed that Hfq is well-conserved in many other bacterial species and is closely related to the Sm family of RNA binding proteins in archaea and eukaryotes (*9*−*12*). During the past several years, *E. coli* Hfq was demonstrated to be important to the regulation of mRNA expression by a number of sRNAs, including DsrA (*13*), OxyS (*10, 14*), RprA (*15*), Spot42 (*11, 16*), RyhB (*17*), and SgrS (*18*). Hfq homologues in other bacterial species appear to play a similar role in sRNA regulation (*19*−*21*).[1]

rpoS was among the first genes shown to be regulated by sRNAs (*22*−*24*). This gene encodes the stationary phase σ factor required to transcribe a group of genes expressed in stationary phase or during growth under stress conditions. *rpoS* is regulated by three sRNAs, 109 nt OxyS (*10, 14*), 87 nt DsrA, and 105 nt RprA. OxyS inhibits *rpoS* mRNA translation, while DsrA and RprA enhance translation in the presence of Hfq (*13*−*15, 24*). In vivo studies of the effect of mutations to DsrA and RprA and their *rpoS* mRNA target site indicated that both sRNAs hybridize to one strand of a predicted duplex segment in *rpoS* mRNA just upstream of the start codon (*15, 25, 26*). This interaction renders accessible the ribosome binding site (RBS) on the other strand. In vitro studies provided direct evidence of the DsrA−*rpoS* mRNA interaction (*27*) and showed that Hfq independently binds to DsrA and a site near the RBS of the *rpoS* mRNA (*27, 28*). Hfq was also shown to enhance binding of DsrA to a 140 nt *rpoS* RNA (*27*), but by an amount (1.8-fold) thought to be small relative to the influence of Hfq on DsrA regulation of *rpoS* mRNA translation in vivo (*4*).

† This work was supported by a Georgia Tech PURA award to N.W. and funding from an IPST grant and the College of Sciences of Georgia Tech.

* To whom correspondence should be addressed. E-mail: roger.wartell@biology.gatech.edu. Phone: (404) 894-8421. Fax: (404) 894-0519.

‡ These authors contributed equally to this work.

[1] Abbreviations: nt, nucleotides; PAGE, polyacrylamide gel electrophoresis; sRNA, small RNA.

10.1021/bi800479p CCC: $40.75
Published on Web 10/01/2008

Hfq has been shown to enhance the binding of a sRNA to its mRNA target for several other sRNA−mRNA pairs in addition to DsrA and *rpoS* mRNA. They include Spot42 and *galK* mRNA (*11*), OxyS and *fhlA* mRNA (*10*), RyhB and *sodB* mRNA (*17*), and SgrS and *ptsG* mRNA (*18*). How Hfq enhances sRNA−mRNA pairing is not fully understood. For DsrA and *rpoS* mRNA as well as some of the RNA pairs mentioned above, in vitro experiments indicate that Hfq is not required for maintenance of stable sRNA−mRNA complexes once they form (*10, 18, 27, 29*). This suggests that Hfq's RNA chaperone activity may alter the conformation of a sRNA or its mRNA target, creating a metastable conformation that enables intermolecular hybridization (*30*). Enhanced hybridization may also result from an Hfq complex sequestering the two RNAs simultaneously, thereby increasing their local concentration and allowing thermal fluctuations or transient binding release by Hfq to drive hybridization.

Evidence that Hfq binding can induce a conformational change to a mRNA or sRNA has been obtained from in vitro nuclease footprinting studies with *sod* mRNA (*17, 30*), *ompA* mRNA (*31*), and OxyS sRNA (*10*). This assay did not, however, indicate a significant alteration to the secondary structure of *rpoS* RNA (*27*). FRET studies showed that Hfq binding to DsrA alters the distance between this RNA's 5′ and 3′ ends (*32*), although it did not produce a significant change to the DsrA CD spectrum (*30*). The studies described above indicate that Hfq binding can alter DsrA conformation, but major distortion in secondary structure is not evident. The role of an Hfq-induced conformational change to RNA in the annealing of a sRNA to its mRNA site remains uncertain.

Three-dimensional crystal structures have been published of the *Staphylococcus aureus* Hfq (*33*), a truncated version of *E. coli* Hfq (residues 4−72) (*34*) and *Pseudomonas aeruginosa* Hfq (*35*). The structures are very similar, each forming a hexameric toroid with an outer diameter of ∼70 Å and a central cavity ∼10 Å wide (Figure 7). The crystal structure of *S. aureus* Hfq with the heptanucleotide AU_5G shows this RNA binding in a circular contour adjacent to the central cavity on Hfq's proximal surface (*33*). Mutagenesis studies indicate that residues along the corresponding contour of *E. coli* Hfq (*28*) as well as residues F39 and R16 on the proximal surface (*36*) influence binding of Hfq to DsrA. Mutations to some residues on the distal surface of *E. coli* Hfq did not have a significant effect on its binding to DsrA or *rpoS* RNA (*28*), but they strongly influenced binding of Hfq to poly(rA) (*28, 36*). A recent investigation showed that residues beyond position 65 on the C-terminal end of *E. coli* Hfq are needed for sRNA regulation in vivo and influence binding of Hfq to *rpoS* mRNA and DsrA in vitro (*32*).

In this work, we examine the binding of *E. coli* Hfq to RprA and two lengths of the *rpoS* mRNA leader region, and the impact of Hfq on the interaction of RrpA with the *rpoS* RNAs. RprA is similar to DsrA in that it binds to the same target region on *rpoS* mRNA, enhances translation, and requires Hfq, yet RprA differs in sequence and length from DsrA. Comparison of the interactions of RprA, Hfq, and *rpoS* RNAs with previous results for DsrA, Hfq, and *rpoS* mRNA can be expected to reveal common features and differences that may shed light on how Hfq enhances the pairing of these sRNAs with their common target site.

Our studies show that Hfq forms two complexes with RprA in a gel shift assay with binding parameters similar to those determined for Hfq and DsrA (*27, 28*). Unlike DsrA, Hfq binding to RprA was inhibited by poly(A) and influenced by Hfq mutations on the distal and proximal surfaces. RprA bound to the two *rpoS* RNAs examined but with different affinities. The 654 nt *rpoS* RNA containing the entire upstream leader sequence showed much weaker binding to RprA than the 210 nt *rpoS* RNA, although both *rpoS* RNAs have the RprA target sequence. Hfq induced a much larger enhancement of RprA binding to the 654 nt *rpoS* RNA compared to the 210 nt *rpoS* RNA. DsrA behaved similar to RprA. This is consistent with a previous in vivo result (*25*) indicating that the full upstream leader sequence of *rpoS* mRNA plays an important role in Hfq activity.

MATERIALS AND METHODS

Plasmid Construction and Transcription of rpoS, RprA, and DsrA RNAs. DNA plasmid templates for *rpoS* RNA transcription were constructed via PCR amplification of segments of the *rpoS* gene in purified *E. coli* K12 DNA. Two primer pairs were used to amplify DNA fragments containing 643 and 199 bp of the *rpoS* mRNA. Subsequent rounds of PCR amplification using standard procedures positioned an EcoRI restriction site and phage T7 promoter sequence upstream of the *rpoS* DNAs and a HindIII restriction site downstream. PCR products of this second round were purified by agarose gel electrophoresis and ligated into the polylinker region of pUC19. The shorter *rpoS* DNA insert created the plasmid designated pUC19rpoS-S, and the plasmid with the longer *rpoS* DNA insert was designated pUC19rpoS-L. Plasmids were transformed into DH5α cells and colonies selected on ampicillin-LB plates. Isolated plasmid DNA was sequenced to verify the inserted DNA sequences.

The runoff transcript from HindIII-digested pUC19rpoS-L includes the start point of *rpoS* mRNA transcription, 565 nt behind the *rpoS* start codon (*37*) and 75 nt in front of this AUG. This 654 nt transcript (rpoS-L) also included six nucleotides (GGGAGA) at the 5′ end from the T7 promoter sequence and five nucleotides from the HindIII site at the 3′ end. The transcribed product from pUC19rpoS-S (rpoS-S) has the same 3′ end as rpoS-L but has only 127 nt of the *rpoS* sequence upstream of the start codon. rpoS-S is 210 nt and includes six nucleotides of the T7 promoter sequence at its 5′ end and the HindIII 3′ end sequence (Figure 2). A 157 nt segment of the *rpoS* mRNA leader region was produced for a limited number of studies by transcribing pUC19rpoS-S digested with the restriction enzyme DraI. This transcript ends 32 nt downstream of the start codon. RprA was produced from a plasmid constructed in a manner similar to that used for the other plasmids. The runoff transcript, 112 nt, added two G residues at the 5′ end from the T7 promoter and five nucleotides due to the HindIII site at the 3′ end to the RprA sequence. Secondary structures predicted using RNA Structure 4.5 (*38*) do not suggest that the additional nucleotides alter folding of the RprA sequence. DsrA was produced from a pUC19-based plasmid using a similar approach. Plasmid was digested by DraI for runoff transcription. The RNA contained the two G residues from the T7 promoter at the 5′ end and the stretch of six A residues at the 3′ end of the DsrA sequence.

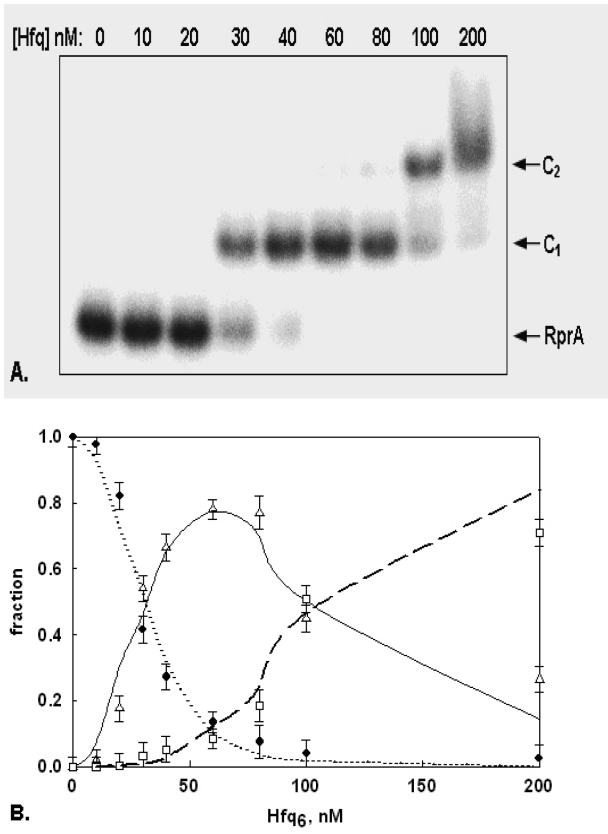

FIGURE 1: (A) Hfq binding to ^{32}P-labeled RprA assessed by a gel mobility shift assay. The Hfq_6 concentration varied from 0 to 200 nM. Hfq−RprA complexes are designated C_1 and C_2. (B) Fraction of total RprA concentration (f) as a function of Hfq_6 concentration in free RprA (◆), complex C_1 (△), and complex C_2 (□) bands. Error bars are based on three experiments. Lines are least-squares fits of the binding model described in eqs 1 and 2 using parameters listed in Table 1: f_o (•••), f_1 (—), f_2 (---).

RNAs were synthesized using the MEGAscript T7 kit (Ambion) according to manufacturer's protocol. RNAs were purified by ammonium acetate precipitation after digestion of the template with DNase (Epicenter). RNAs were characterized by native and denaturing gel electrophoresis, and their concentrations were determined by UV absorbance and a RiboGreen fluorescence assay (Invitrogen Inc.). ^{32}P labeling of the RNAs was carried out using standard protocols. RNA was dephosphorylated with shrimp alkaline phosphatase, radioactively labeled at the 5′ end with [γ-^{32}P]ATP and T4 polynucleotide kinase, and purified by gel electrophoresis followed by elution from gel slices in 0.5 M ammonium acetate and ethanol precipitation. RNAs were dissolved in DEPC-treated water or 2 mM sodium citrate and 0.1 mM EDTA and stored at −70 °C.

Purification and Characterization of Wild-Type (wt) and Mutant Hfq. The Impact-CN intein system (New England Biolabs) was used to purify Hfq proteins as previously described (*36*). The *E. coli hfq* gene was amplified by PCR using *E. coli* chromosomal DNA as the template. PCR products were digested with SapI and cloned into a SapI−SmaI-digested pTYB11 plasmid. Protein purification was carried out according to the recommendation of the manufacturer using strain ER2566. Cell lysis was carried out using a French press. The cell lysate was centrifuged and the supernatant loaded onto a chitin column. The column was extensively washed with the lysis/wash buffer of 20 mM Tris (pH 8.3) and 1 M NaCl prior to incubation of the column with this buffer and 40 mM dithiothreitol. The eluted protein was concentrated and buffer-exchanged to 0.5 M NaCl and 20 mM Tris at pH 8.3 using centrifugation filtration units.

Mutant Hfq proteins were produced as described previously from plasmids containing mutant hfq genes generated using the QuikChange mutagenesis kit from Stratagene Inc. (*36*). Plasmid constructs were verified by DNA sequencing. The same procedure used to purify wt Hfq was used to purify the mutant proteins. All proteins showed the 11 kDa monomer band by sodium dodecyl sulfate−polyacrylamide gel electrophoresis (SDS−PAGE) with the purity estimated to be ∼95% from Coomassie blue staining. Characterization was also carried out using analytical sedimentation velocity centrifugation in 0.5 M NaCl and 20 mM Tris (pH 8.3), circular dichroism, and UV absorbance spectra. The absorbance ratio of A_{274}/A_{250} indicated less than 5% of the contaminating nucleic acid.

RNase H Degradation Assay. DNA oligonucleotide probes were purchased commercially and dissolved in TE and their concentrations evaluated by UV absorbance. The sequences of the five probes in the 5′ to 3′ direction were as follows: (1) GCTCCTAC, (2) CGATTTAT, (3) GCAAATAAC, (4) GACGGAAC, and (5) CGCAGCGG. A master mixture (60 μL) containing RNA and *E. coli* RNase H1 (USB) was preincubated for 15 min at 25 °C in RNase H buffer with 0.2 unit of prime RNase inhibitor. The RNase H buffer contained 20 mM KCl, 10 mM $MgCl_2$, 20 mM Tris (pH 7.5), 0.1 mM EDTA, and 0.1 mM DTT. Seven microliters from this mixture was added to each reaction tube with 3 μL of a given DNA probe in RNase H buffer. The final DNA and RNA concentrations were 15 and 1.5 μM, respectively, in each tube. Each reaction mixture was incubated at 37 °C for 15 min; 30% glycerol loading buffer was mixed directly to the samples which were heated for 1 min at 80 °C, placed in ice, and then run immediately into an 8% polyacrylamide gel for rpoS-S RNA and 5% gel for rpoS-L RNA. For rpoS-L, nucleic acid bands were visualized by staining the gel with SYBR Gold (Invitrogen). For rpoS-S, the master mixture contained ^{32}P-labeled RNA as a marker. Gels were scanned and analyzed using a Fujifilm Image Reader FLA-3000 in fluorescence or IP mode. The percentage of RNase H-induced degradation of RNA was evaluated by comparing the band intensities of the full-length RNAs with and without DNA probes.

Electrophoretic Gel Mobility Shift Assay. Mixtures for binding reactions between wt Hfq and mutant Hfq and ^{32}P-labeled rpoS-S or RprA RNAs were prepared in 15 μL volumes. Five microliters of 12 nM RNA (final concentration of 4 nM) was mixed with 7.5 μL of an Hfq solution to give the appropriate Hfq concentration and 2.5 μL of loading buffer (0.25% bromophenol blue and 30% glycerol). The final reaction solvent consisted of 20 mM Tris-HCl (pH 8.0), 100 mM NH_4Cl, 50 mM NaCl, 50 mM KCl, and 5% glycerol. The RNA and Hfq solutions were prepared in the solvent described above except for the glycerol. Reaction mixtures were incubated for 5 min at 37 °C and then for 10 min at room temperature (25 °C). For experiments in which poly(A) or A_{18} was added, an additional 10 min incubation at 25 °C followed the additions prior to loading samples.

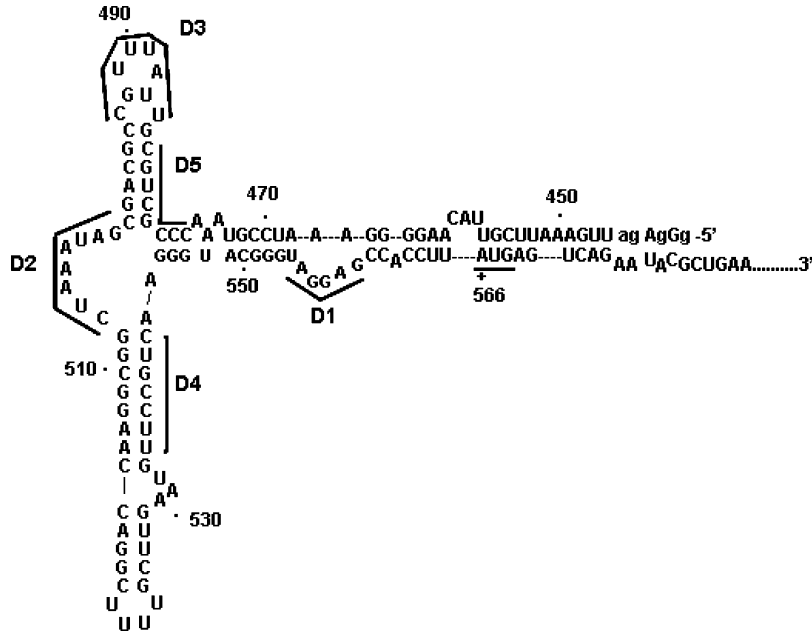

FIGURE 2: Predicted secondary structure of rpoS-S RNA except for 58 nt at the 3′ end. The AUG start codon is underlined. Numbers designate base positions from the transcription start point. Segments D1−D5 are target locations of DNA probes used in the RNase H assay.

Samples were analyzed by electrophoresis on native 5% polyacrylamide gels [29:1 (w/w) acrylamide/bisacrylamide] gels with 3% glycerol in 0.5× TBE. Gels were run at 80−100 V and room temperature. The fraction of ^{32}P-labeled RNA that was free or in Hfq·RNA complexes was determined from the counts in each band relative to the total counts in each lane. Binding of Hfq to rpoS-L RNA was carried out in a similar manner except that SYBR Gold stain was employed to image and analyze Hfq binding. Labeling of rpoS-L with ^{32}P was also carried out, but degradation of this longer RNA during purification compromised its use.

Association of rpoS-S or rpoS-L RNA with ^{32}P-labeled RprA in the absence or presence of Hfq was evaluated using the same reaction volume and buffer described above. Varying concentrations of unlabeled rpoS-S or rpoS-L RNA were added to 4 nM RprA and incubated for 60 min at 25 °C prior to electrophoresis at 4 °C on a native 5% polyacrylamide gel. Gels were run at 100−115 V for 60−90 min and analyzed using a Fujifilm Image Reader FLA-3000.

Evaluation of Binding Constants. Equilibrium binding parameters describing the interaction of Hfq with RprA were determined from a least-squares fit of the gel shift data to a model that assumed Hfq_6 may cooperatively bind to two different independent sites on RprA. The fraction of ^{32}P-labeled RprA that was free or in observed complexes C_1 and C_2 (f_o, f_1, and f_2, respectively) was calculated from the counts in each band relative to the total counts in the lane. The experimental fractions are related to the model by the equations

$$f_1=([H]/K_1)^{n_1}/Q_2 \quad (1a)$$

$$f_2=([H]/K_1)^{n_1}([H]/K_2)^{n_2}/Q_2 \quad (1b)$$

$$f_o=1-f_2-f_1 \quad (1c)$$

with

$$Q_2=1+([H]/K_1)^{n_1}+([H]/K_1)^{n_1}([H]/K_2)^{n_2} \quad (2)$$

where [H] is the free Hfq_6 concentration, K_1 and K_2 are the equilibrium dissociation constants for Hfq binding to the first and second sites, respectively, and n_i is the Hill cooperativity coefficient for binding site i. [H] was determined from the equation

$$[H]=[H_T]-n_1f_1[R_T]-(n_1+n_2)f_2[R_T] \quad (3)$$

where $[H_T]$ and $[R_T]$ are the total concentrations of Hfq_6 and RprA, respectively. This model is the same as that employed by Lease and Woodson (*27*), except that it considers the possibility of different n values for the two sites and accounts for the Hfq concentration in terms of moles of hexamer rather than monomer. Experimental values of f_1, f_2, $[H_T]$, and R_T and an assumed (n_1,n_2) pair were employed in eq 3 to calculate [H] values which were then employed in eqs 1 and 2 to solve for K_1 and K_2 by a nonlinear least-squares fit to the data (Sigma Plot, SPSS Inc.). The process was iterated varying (n_1,n_2) in 0.1 increments between 1 and 3. Solutions were assessed for convergence, and the best fit was determined from the maximum correlation coefficient R^2.

Hfq binding to rpoS-S was analyzed using a similar approach with a model that assumed Hfq_6 may cooperatively bind to five independent sites. The Hill coefficient for all sites was assumed to be the same ($n_i = n$). The fractions of rpoS-S in the five complexes were related to the binding parameters by equations similar to eq 1:

$$f_j=\prod_{i=1}^{j}([H]/K_i)^{n_i}/Q_5, \text{ for } j=1-5 \quad (4a)$$

$$Q_5=1+\sum_{j=1}^{5}\prod_{i=1}^{j}([H]/K_i)^{n_i} \quad (4b)$$

Unlike the gel shift results with RpoS-S, Hfq binding to RpoS-L RNA did not display complexes as discrete bands. A broad band was observed that decreased in mobility with an increase in Hfq concentration (Figure 4B). To quantify

Table 1: Equilibrium Binding Parameters of Hfq−RNA and RprA−*rpoS* RNA Complexes[a]

components	no. of Hfq−RNA gel bands observed	K_d values (nM)	n
Hfq and RprA	2	24, 96	2.1−2.8
Hfq and rpoS-S	5	50, 66, 89, 92, 97	2.2−2.6
Hfq and rpoS-L		35 ± 10[b]	
RprA and rpoS-S		120 ± 20[b]	
RprA and rpoS-L		2500 ± 300[b]	

[a] Parameters of Hfq binding RprA and rpoS-S were obtained by a least-squares fit of gel shift data to cooperative binding models described by eqs 1−4. K_d values are the equilibrium dissociation constants for complexes in the order at which they appeared with an increasing Hfq_6 concentration. n is the Hill cooperative binding parameter. [b] Apparent K_d values for Hfq binding to rpoS-L and RprA binding to rpoS-S or rpoS-L. Evaluated using the model described by eqs 5 and 6. Values are averaged from three experiments. Reaction mixtures were incubated at 25 °C.

the affinity of Hfq_6 for this RNA, a simplified analysis was employed that considers the RNA to be in two states, free and bound:

$$nH + R \leftrightarrow H_n \cdot R \quad (5)$$

where R represents RpoS-L RNA and n represents an average stoichiometry of the complexes. The dissociation constant K of eq 5 can be related to the fraction of unbound or free RNA ($f = [R]/[R_T]$) by the following equation (*39*):

$$\log[(1 - f)/f] = \log K + n \log[H] \quad (6)$$

where K is related to the geometric mean of the n intrinsic binding constants that lead to $H_n \cdot R$; i.e., $K = (K_d)^n$, where $K_d = (K_1K_2...K_n)^{1/n}$. The intercept of the plot of n^{-1} $\log[(1 - f)/f]$ versus $\log[H]$ yields K_d, a value that reflects the mean of the binding constants for the n binding steps leading to $H_n \cdot R$.

Comparison of the binding affinity of various mutant and wild-type Hfq's for RprA and rpoS-S also employed the simplified analysis described above. This approach was used since the weak affinity of some mutant Hfq's produced broad, sometimes overlapping complex bands, making them difficult to quantify. This compromised the ability to compare all mutant Hfq's using the more detailed analysis described by eqs 1−4.

RESULTS

Hfq Binding to RprA. Immunoprecipitation experiments have shown that Hfq binds to RprA (*5*); however, the affinity of Hfq for this sRNA has not been previously investigated. Figure 1A shows a gel mobility shift experiment of 4 nM RprA with varying amounts of Hfq. Two Hfq−RprA complexes are observed (C_1 and C_2). Their relative mobility implies that more Hfq is bound to the second complex. Association and dissociation of Hfq with RprA were rapid. Experiments showed all of the RprA shifted to the C_1 band within ~30 s after addition of 40 nM Hfq_6 to 4 nM RprA, and preformed complex C_1 dissociated completely to free RprA within ~30 s after addition of saturating amounts of poly-rU to trap free Hfq (data not shown). This rapid association and dissociation behavior is similar to what was observed for DsrA (*27*).

Equilibrium dissociation constants for the formation of complexes C_1 and C_2 were evaluated using the Hill cooperative binding model (eqs 1−3). This model assumes that one or more Hfq_6 units may bind RprA to form complex C_1 and additional Hfq_6 bind C_1 to form complex C_2. The least-squares fit yielded equilibrium dissociation constants (K_1 = 24 ± 3 nM and K_2 = 96 ± 9 nM) with Hill coefficients (n_1 and n_2) ranging from 2.1 to ≤2.8 (Figure 1B). The correlation coefficient R^2 was 0.945 ± 0.02 in this range. Values of n_1 and n_2 outside this range reduced the quality of the fit. If we fixed n_1 and n_2 to 1, we obtained an R^2 of 0.77. Thus, approximately two Hfq_6 units bound to each site gave a markedly better fit to the data than one Hfq_6 per site. Mixing increasing amounts of Hfq_6 with 100 nM RprA, a concentration above the K_d of complex C_1, saturated the C_1 complex at a 2:1 molar ratio of Hfq_6 to RprA (Figure S1 of the Supporting Information), consistent with the model fitting analysis.

rpoS mRNA Leader Sequence and Characteristics of RBS Secondary Structure. Hfq has previously been shown to bind to a portion of the *rpoS* mRNA leader sequence that surrounds the AUG start codon (*27, 28*). The rpoS RNAs were ~140 nt long extending from position −134 to +3 or from position −128 to +12 relative to the start codon and predicted to fold up in the manner displayed in Figure 2. Since RprA and DsrA bind to a sequence within this region (*15, 26*), and DsrA binding makes the ribosome binding site (RBS) accessible (*27*), this ~140 nt region is essential for Hfq−sRNA stimulated translation. If this *rpoS* RNA region is all that is required for the functional interactions of RprA and Hfq, upstream or downstream sequences are not expected to have a strong influence. However, in vivo studies indicate that the *rpoS* mRNA sequence more than 220 nt upstream of the start codon is required for regulation by Hfq (*25*).

To explore the influence of the sequence upstream and downstream of the RBS on interaction of Hfq with *rpoS* mRNA and RprA−*rpoS* RNA pairing in vitro, two transcripts of the *rpoS* mRNA leader region were synthesized. rpoS-L RNA contains the start point of transcription 565 nt upstream of the start codon and 75 nt downstream from this AUG (Materials and Methods). rpoS-S RNA includes 127 nt of the *rpoS* mRNA sequence upstream of the start codon and has the same downstream sequence as rpoS-L. An RNase H assay was employed to examine if the secondary structure in the vicinity of the RBS was preserved in these two RNAs.

The predicted secondary structure of the sequence surrounding the RBS of the *rpoS* mRNA is shown in Figure 2 along with the location of five sites targeted by cDNA probes in the RNase H assay. RNase H degradation of rpoS-S and rpoS-L RNAs with the five DNA probes is shown in Figure 3. Probes 1 and 3 target sites predicted to be unpaired, and both induce significant RNA degradation. Probe 1 induced approximately 90 ± 7% degradation of both RNAs, while probe 3 produced 57 ± 10% degradation of rpoS-S RNA and 30 ± 7% degradation of rpoS-L RNA. DNA probes 4 and 5 target sites are predicted to be base paired, and as expected, both probes produced very small amounts of degradation in both RNAs. Probe 2 targets a site predicted to form an unpaired loop; however, little degradation was observed for both RNAs. The DNA−RNA hybrid expected to be formed by probe 2 has the lowest predicted T_m among the DNA−RNA hybrids. This factor and/or the RNA three-dimensional structure may account for the small amount of degradation produced. The results from this assay indicate

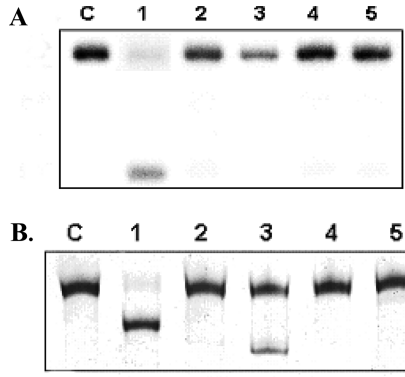

Probe:	rpoS-S RNA % degradation(±7%) :	rpoS-L RNA % degradation (±7%):
1	91	85
2	6	9
3	57	30
4	6	4
5	8	10

FIGURE 3: Results of the RNase H assay of rpoS-S and rpoS-L using five DNA oligomer probes (see Materials and Methods). (A) Degradation of rpoS-S: C, control (no DNA); lanes 1−5, degradation with corresponding DNA probes 1−5, respectively. (B) Degradation of rpoS-L: C, control (no DNA); lanes 1−5, degradation with corresponding DNA probes 1−5, respectively.

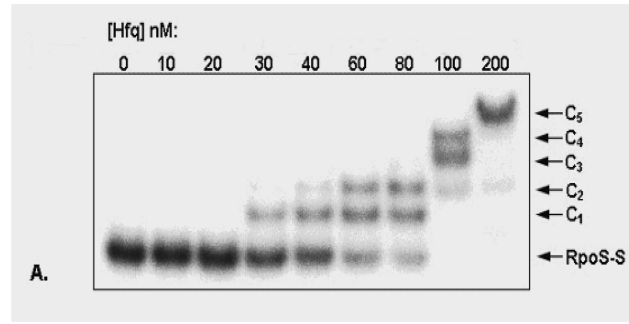

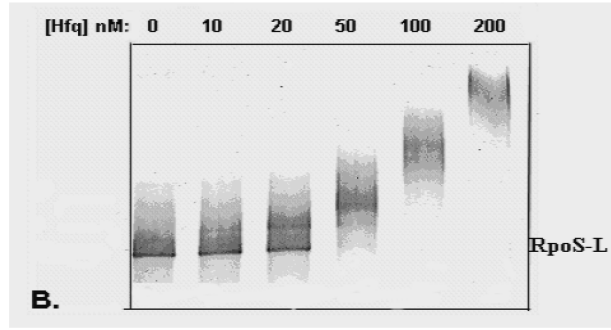

FIGURE 4: Hfq binding to rpoS-S (A) and rpos-L (B) assessed by gel mobility shift assays. The Hfq_6 concentration varied from 0 to 200 nM. Hfq−rpoS-S complexes are designated C_1−C_5. An 8% polyacrylamide gel was employed for rpoS-S and a 5% polyacrylamide gel for rpoS-L.

that the secondary structure surrounding the RBS is similar for rpoS-S and rpoS-L RNAs.

Hfq Binding to rpoS-S and rpoS-L RNAs. Electrophoretic gel mobility shift assays were carried out to determine the binding affinity of Hfq for rpoS-S and rpoS-L RNAs. When 4 nM rpoS-S RNA was titrated with increasing amounts of Hfq, five discrete bands were observed (Figure 3B). The faster mobility bands decreased in intensity as the slower mobility bands appeared. Increasing the rpoS-S RNA concentration resulted in an increase of the faster mobility complexes at the expense of the slower complexes (data not shown). Both observations are consistent with the complexes (C_i, $i = 1-5$) representing one rpoS-S RNA with increasing numbers of bound Hfq_6 per RNA. The data were fit to the model described in Materials and Methods associated with eq 4. The evaluated equilibrium constants for the five complexes (C_1−C_5) were 50, 66, 89, 92, and 97 nM (±10%), respectively, with an n of 2.4. The correlation coefficient R^2 was 0.93. Hill coefficients ranging from 2.2 to 2.6 produced similar results for the K_i values and R^2. If n was set equal to 1, R^2 was lower (0.875) and the least-squares solution for K_1−K_5 was physically unrealistic. The binding constants were 91, 63, 134, 119, and 63 nM, respectively, no longer increasing in value in the order of appearance of the complexes. Thus, approximately two Hfq_6 units per site produced a better fit to the rpoS-S RNA gel shift data than one Hfq_6 per site.

Hfq binding to rpoS-L RNA is shown in Figure 3B. As the ratio of Hfq_6 to rpoS-L RNA increased, the complex(es) migrated as a broad band with decreasing mobility. Since discrete complex bands were not observed, the data were analyzed using a binding model that considered rpoS-L RNA as either free or bound (i.e., eqs 5 and 6). The apparent K_d was estimated to be 35 ± 10 nM from three experiments, indicating a slightly greater affinity than the strongest binding site (50 nM) determined for rpoS-S RNA.

These results show that Hfq binds to the rpoS-S and rpoS-L RNAs with similar affinity. Multiple discrete complexes are formed with the 210 nt rpoS-S RNA, and the decreasing mobility of the Hfq−rpoS-L RNA band with an increasing level of Hfq_6 suggests that multiple Hfq_6−RNA complexes also form for this RNA. The inability to resolve discrete bands may be attributed to this RNA's longer length and/or the overlapping mobility of different complexes. More than one discrete Hfq−RNA complex has been previously observed in gel shift experiments for several sRNAs or mRNA targets of Hfq (*10, 27, 28, 40*). Unless this behavior is an artifact of the gel conditions, it indicates Hfq_6 either commonly binds to several different sites on its RNA target molecules, cooperatively associates with RNA-bound Hfq_6, or both.

Binding of RprA to rpoS-S and rpoS-L RNAs and the Influence of Hfq. In vivo studies indicate that RprA stimulation of RpoS translation is enhanced by Hfq (*15*), presumably by Hfq promoting the binding of RprA to its rpoS mRNA target site. In this work, we examine the equilibrium binding of RprA to the core rpoS RNA (rpoS-S) and the full leader region of the *rpoS* mRNA (rpoS-L) at 25 °C and the influence of Hfq on these interactions. Figure 5A shows a polyacrylamide gel of RprA binding to rpoS-S RNA in the absence of Hfq. The equilibrium dissociation constant for forming the RprA·rpoS-S complex was ~120 ± 20 nM based on three trials. When a 157 nt portion of rpoS-S RNA was employed, which was missing 53 nt at the 3′ end, the K_d value was similar (data not shown). Figure 5B shows a similar gel shift experiment of RprA binding to rpoS-L RNA.

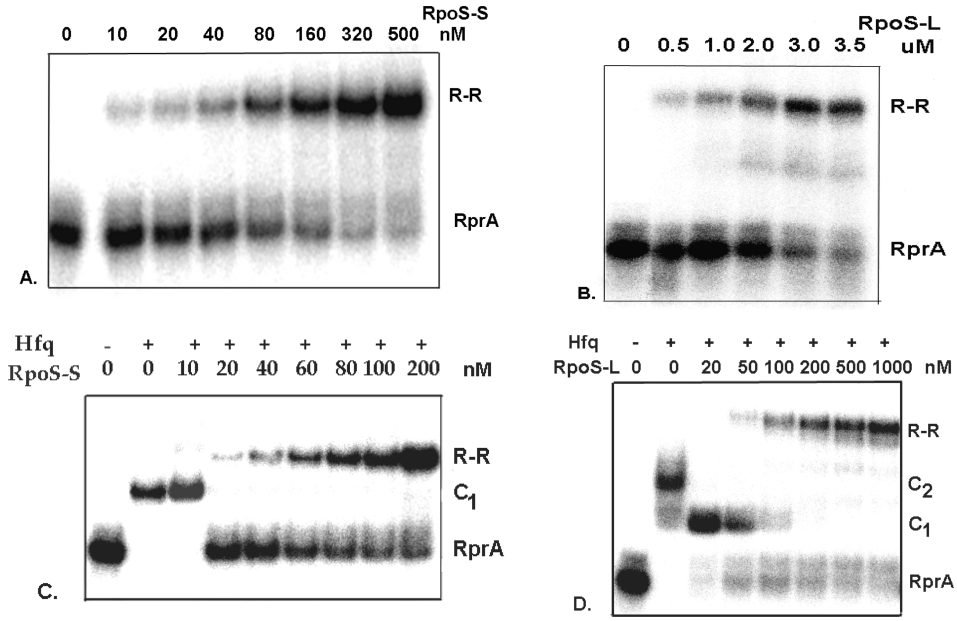

FIGURE 5: (A) Binding of rpoS-S to ^{32}P-labeled RprA. rpoS-S (0−500 nM) was added to 4 nM RprA and run in 5% polyacryamide gels (see Materials and Methods). R-R denotes the RprA−rpoS-S complex. (B) Binding of rpoS-L to ^{32}P-labeled RprA. rpoS-L (0−3.5 μM) was added to 4 nM RprA and run on 5% polyacrylamide gels. (C) Binding of rpoS-S to RprA as in panel A in the absence (−) or presence (+) of 50 nM Hfq_6. C_1 denotes the strong Hfq−RprA complex of Figure 1. (D) Binding of rpoS-L to RprA as in panel B in the absence (−) or presence (+) of 200 nM Hfq_6.

The stability of the RprA·rpoS-L RNA complex was considerably weaker with a K_d of ~2500 nM. The complete upstream leader sequence of rpoS-L RNA apparently inhibits RprA binding.

The influence of Hfq on the binding of RprA to rpoS-S and rpoS-L RNAs was examined next. Hfq_6 (40 nM) was mixed with 4 nM RprA, and varying concentrations of rpoS-S RNA were added (Figure 5C). Hfq_6 forms the strong binding complex with RprA (C_1) in the absence of rpoS-S RNA. As rpoS-S RNA was added, the intensity of the free RprA band initially increased and then decreased as the RprA·rpoS-S RNA band formed. The latter band was assigned to the RprA·rpoS-S RNA complex since its mobility relative to free RprA was the same as in Figure 5A. The initial increase in the level of free RprA indicates that rpoS-S RNA can displace Hfq from the RprA−Hfq complex. Although Hfq has a greater affinity for RprA than rpoS-S RNA (Table 1), the higher concentration of rpoS-S RNA versus RprA overcomes this difference in affinity. The rpoS-S RNA concentration at which the intensity of the RprA·rpoS-S RNA band equaled the intensity of the free RprA band was 80 ± 20 nM. The stability of the RprA·rpoS-S RNA complex increased by ~1.5-fold in the presence of 40 nM Hfq_6. Figure 5D shows the effect of 200 nM Hfq_6 on the formation of the RprA·rpoS-L RNA complex. The apparent binding constant of RprA for rpoS-L RNA was reduced to ~75 nM, a ~30-fold increase in the stability of RprA for the full-length rpoS mRNA leader region in the presence of Hfq_6.

In addition to the much larger effect of Hfq on the binding of RprA to RpoS-L RNA compared with RprA binding rpoS-S RNA, several points are worth noting in the experiments described above. RprA binding to both rpoS RNAs in the absence of Hfq required incubation times of approximately 40 min to ensure equilibrium. When Hfq was present, the time required to reach equilibrium was reduced (Figure S2 of the Supporting Information). Thus, Hfq enhancement of the stability of the RNA hybrids correlates with an increased association rate. A more detailed analysis of association−dissociation kinetics is being investigated. The concentrations of Hfq_6 that were employed in panels C and D of Figure 5 optimized formation of the RprA·rpoS RNA complex, i.e., gave the lowest apparent equilibrium dissociation constants. If >100 nM Hfq_6 was incubated with the 4 nM RprA prior to addition of rpoS-S RNA, formation of the RprA·rpoS-S RNA complex was inhibited. A similar result was observed if >200 nM Hfq_6 was employed in the rpoS-L RNA titration of RprA (data not shown). This suggests that excess Hfq sequesters the added rpoS RNA or binds to secondary RprA sites inhibiting formation of the RprA·rpoS RNA complex.

A number of coupled reactions govern the distribution of RprA in the presence of rpoS RNA and Hfq. We have examined three of them as independent reactions: Hfq binding to each RNA and RprA binding to rpoS RNA. A fourth reaction to consider is Hfq binding to the RprA·rpoS RNA complex to form a ternary complex. Previous work showed that Hfq can form a ternary complex with DsrA and rpoS RNA (*27*). Figure 6 illustrates the influence of Hfq on the preformed RprA·rpoS-S RNA complex.

Adding up to 40 nM Hfq_6 reduced the amount of RprA·rpoS-S RNA complex by ~15%. A small amount of the Hfq_6·RprA band was detected (~5%), but no ternary complex was observed. Hfq may also be binding to RpoS-S RNA which is at a substantially higher concentration than RprA and is not visible in the gel. The ability of Hfq to dissociate a truncated model of the DsrA·rpoS RNA complex and shift the equilibrium to Hfq bound to the individual RNAs was previously observed (*41*). When ≥80 nM Hfq_6 was added, a small amount of the ternary Hfq·RprA·rpoS-S complex was observed and the intensity of the Hfq_6·RprA complex (C_1) increased.

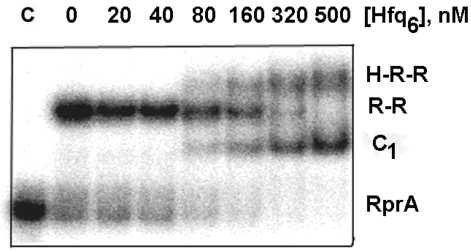

FIGURE 6: Effect of Hfq_6 on the preformed rpoS-S·RprA complex. The first lane is control (C) with 4 nM ^{32}P-labeled RprA. Other lanes included 4 nM RprA preincubated with 200 nM rpoS-S to form the RprA−rpoS-S complex (R-R). Hfq_6 (0−500 nM) was added and incubated for 10 min prior to loading in a 5% polyacrylamide gel. C_1 denotes a strong Hfq−RprA complex and H-R-R the Hfq−RprA−rpoS-S complex.

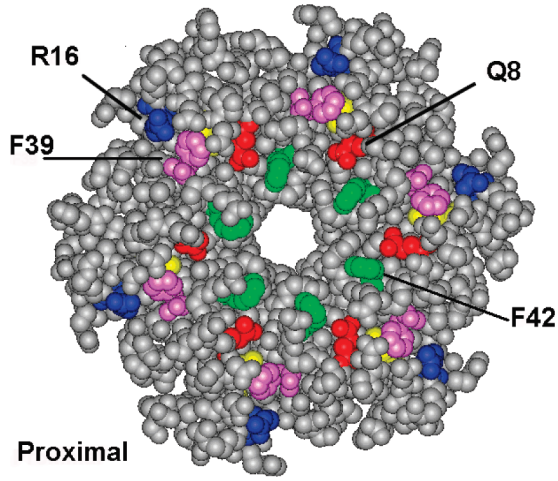

FIGURE 7: Space filling model of the proximal surface of the *E. coli* Hfq hexamer core showing the location of four residues mutated to alanine: F42A (green), Q8A (red), F39A (purple), and R16A (blue).

Although the affinity of Hfq for the RprA·rpoS RNA complex could not be determined directly, the ternary complex appears to be less stable than the Hfq_6·RprA or Hfq_6·RpoS RNA complex. Figure 6 shows that the ternary complex is observed only when the Hfq_6 concentration is high relative to those of RprA and rpoS-S RNA. The effect of Hfq_6 concentration on preformed RprA·rpoS-L complexes gave similar results (data not shown). It may be worth noting that Hfq_6 rapidly associates with the RprA·rpoS-S RNA complex (within ~30 s) and that the ternary complex dissociates within 30 s to the RprA·rpo-S RNA complex and Hfq_6 when challenged with saturating amounts of poly(U) (data not shown). This rapid association and dissociation of Hfq with the RprA·rpoS RNA hybrid is similar to observations made with the DsrA·rpoS RNA complex (*27*).

Effect of Hfq Mutations on RprA and rpoS-S Binding. The effect of mutations to Hfq on its ability to bind RprA and rpoS-S was examined by the gel mobility shift assay. Five mutant proteins, designated Hfq-F42A, Hfq-F39A, Hfq-R16A, Hfq-Q8A, and Hfq-Y25A, were employed. The first four proteins have mutations on the proximal face of Hfq, while Hfq-Y25A has substitutions on the distal surface (Figure 7). Figure 8A shows representative gel shift experiments of three mutant Hfq proteins with RprA, and Figure 8B displays the experimental data on the fraction of free

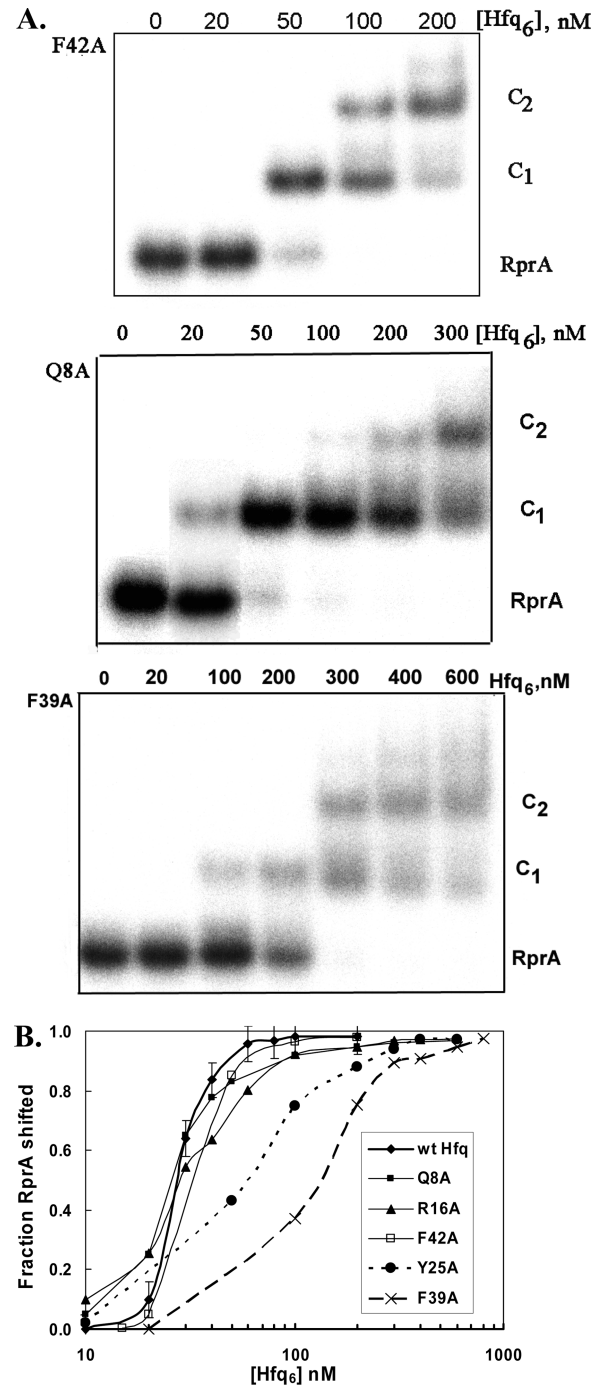

FIGURE 8: (A) Binding of three Hfq mutants to RprA assessed by the gel shift assay. (B) Fraction of total RprA shifted from free to bound complexes as a function of Hfq_6 concentration for wt and five Hfq mutants. Error bars are shown only for wtHfq data for clarity.

RprA shifted (F_B) as a function of Hfq concentration. Each mutant Hfq protein formed two complexes with RprA but with varying affinities. Since the weak affinity of some of the mutant Hfq compounds produced smeared bands making intensities difficult to evaluate, apparent K_d values were determined using the simplified binding model described by eqs 5 and 6 (Figure S3 of the Supporting Information). Hfq-Q8A, Hfq-R16A, and Hfq-F42A gave apparent K_d values within 50% of that of wt Hfq. Mutants Hfq-Y25A and Hfq-F39A exhibited weaker affinities with apparent K_d values 3.5- and 5.0-fold higher than that of wt Hfq, respectively.

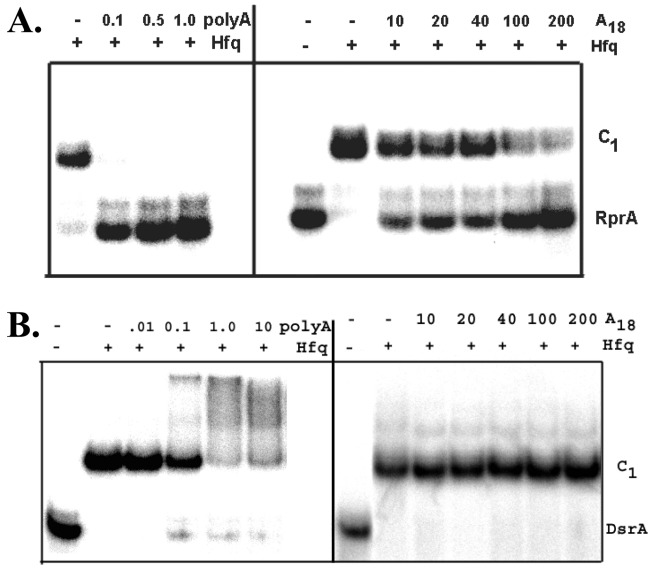

FIGURE 9: (A) Effect of poly(A) and A_{18} on the Hfq−RprA complex. Hfq_6 (50 nM) was incubated with 4 nM ^{32}P-labeled RprA to form complex C_1 (lanes + for Hfq). Poly(A) or A_{18} was then added, and solutions were incubated for an additional 10 min prior to being run on 5% polyacrylamide gels. Four lanes on the left: C_1 complex with no poly(A) (−) and with 0.1, 0.5, and 1.0 ng/μL poly(A) (final concentrations). Seven lanes on the right: RprA alone, C_1 complex, and C_1 complex with A_{18} added to give a concentration of 10−200 nM. (B) Same experiments as described in panel A with DsrA replacing RprA.

Previous work showed that poly(A) and oligomers A_n (n = 18 or 27) bind to the distal Hfq surface (*28, 36*). Competition experiments were carried out in which poly(A) or A_{18} was added to the preformed C_1 complex of Hfq·RprA. Both A_{18} and poly(A) displaced Hfq from RprA (Figure 9A). This result contrasts with previous work that showed that the addition of poly(A) or A_{27} to the Hfq·DsrA complex did not release DsrA and produced "supershifted" gel bands indicative of simultaneous binding of poly(A) and DsrA to Hfq (*28, 30*). Competing poly(A) or A_{18} with the Hfq·DsrA complex under our experimental conditions confirmed this behavior (Figure 9B). DsrA was not released in either case. The Hfq·DsrA band was shifted to lower mobility by poly(A), although not noticeably so by A_{18} which is shorter than the A_{27} used previously (*30*).

Figure 10 shows three representative gel shift experiments of the mutant Hfq proteins binding to rpoS-S and plots of the experimental fraction of rpoS-S shifted as a function of Hfq concentration. Apparent dissociation constants of the mutant Hfq were evaluated using the simplified binding model described by eqs 5 and 6 (Figure S4 of the Supporting Information). Hfq-F42A, Hfq-Q8A, and Hfq-Y25A exhibited relatively well defined shifted bands, and their apparent K_d values were within 2-fold of the wt Hfq value for rpoS-S. Gel shift experiments with the other Hfq mutants produced broader protein·RNA bands and weaker binding. This is illustrated in Figure 10A for Hfq-R16A. The F39A and R16A mutations reduced the apparent K_d by 3.2-fold compared to that of wt Hfq. We note that our results for Hfq-Q8A and Hfq-Y25A differ somewhat from those of a previous study of these mutant Hfqs that reported affinities for *rpoS* RNA slightly higher than that of wt Hfq (*28*). These differences may be due to differences in reaction conditions or protein preparations and are in any case relatively small.

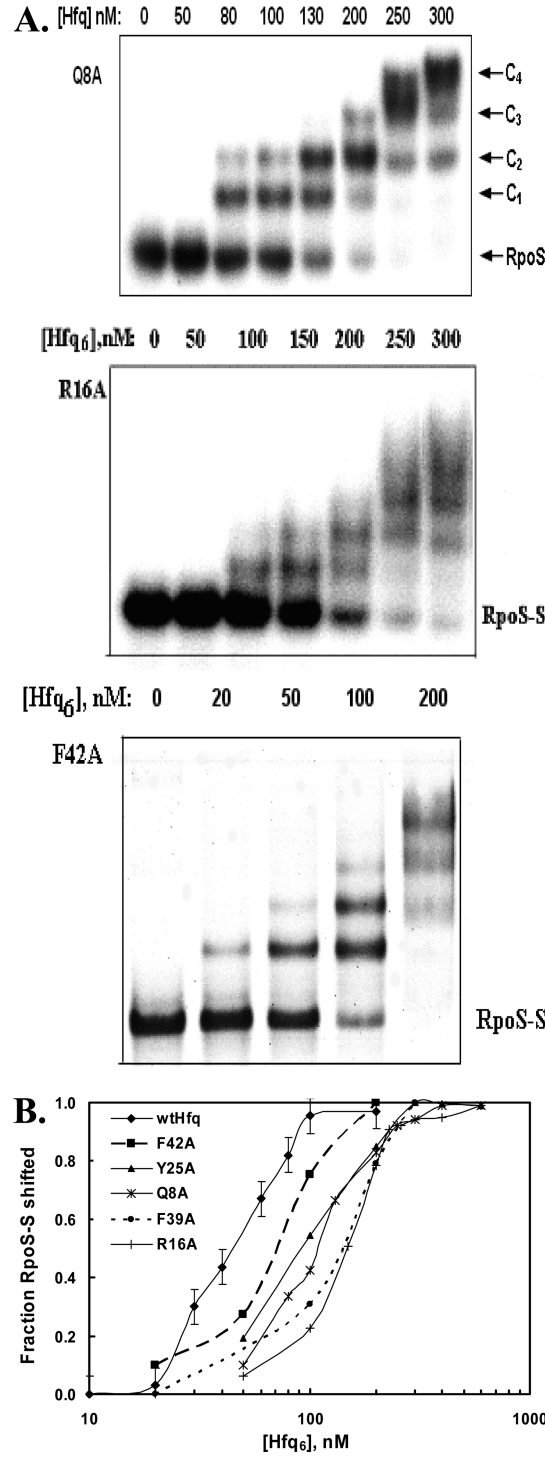

FIGURE 10: (A) Binding of three mutant Hfq forms to rpoS-S assessed by a gel shift assay. (B) Fraction of total rpoS-S shifted from free band to bound complexes as a function of Hfq_6 concentration for wt and five mutant Hfq's. Error bars shown only for wtHfq data.

DISCUSSION

Genetic studies have shown that RprA and DsrA enhance translation of the *rpoS* mRNA in the presence of Hfq. Mutations in the sRNAs and compensating mutations in the *rpoS* mRNA provide compelling evidence that both sRNAs bind *rpoS* mRNA between nucleotides 452 and 473 paired to the RBS in Figure 2 (*15, 26*). The sequence depicted in Figure 2 is undoubtedly important for in vivo regulation of

rpoS. However, as previously noted (*4*), addition of Hfq to this *rpoS* RNA region and DsrA enhanced association of these RNAs by only 1.8-fold (*27*) compared to the 30-fold effect of Hfq on DsrA-mediated regulation of RpoS in vivo (*13*). This implies additional factors may be involved in the regulation of *rpoS* translation.

Our in vitro results point to an additional factor in the regulation of *rpoS* by Hfq and RprA. Hfq enhanced RprA binding to the 210 nt rpoS-S RNA by ~1.5-fold, similar to the enhancement observed for DsrA and a 140 nt rpoS RNA (*27*). However, when the entire *rpoS* leader region (rpoS-L) was examined, Hfq enhanced RprA binding by ~30-fold. This strong influence of the 5′ end of the *rpoS* transcript is qualitatively consistent with in vivo results of Cunning et al. (*25*). These authors showed that when the 5′ end of the *rpoS* transcript was deleted such that it still retained 220 nt upstream of the start codon, which includes the RprA/DsrA binding region, it was not regulated by Hfq. They proposed that a site near the 5′ end of the *rpoS* transcript may be involved in translational regulation.

The difference in the affinity of RprA for rpoS-S versus rpoS-L RNA in the absence of Hfq indicates that the initial ~430 nt of the *rpoS* transcript inhibits RprA binding over and above the inhibitory secondary structure around the RBS. Since the RNase H degradation assay did not indicate a major difference in secondary structure in the vicinity of the RBS for rpoS-S versus rpoS-L RNAs (Figure 3), the 5′ end of this transcript does not appear to propagate a major rearrangement of secondary structure in the RBS region. We hypothesize that intramolecular tertiary interaction involving a site near the 5′ end of the *rpoS* transcript and a site near the RBS inhibits RprA pairing and Hfq overcomes this inhibition. The effect of Hfq on DsrA binding to rpoS-S and rpos-L RNAs yields results similar to that observed with RprA (Figure S5). DsrA binds rpoS-S RNA with greater affinity than to rpoS-L RNA (7.5-fold), and Hfq enhances the apparent K_d of DsrA binding to rpoS-L RNA to a greater extent than to rpoS-S RNA (30-fold vs 1.5-fold).

The 30-fold enhancement of RprA·rpoS-L RNA binding induced by Hfq in vitro is considerably larger than the 6.7-fold enhancement by Hfq determined in vivo for RprA-mediated translation of a *rpoS-lac* fusion gene (*15*). However, the temperature of our experiments, 25 °C, differs from the conditions used in the in vivo study (37 °C). When we reexamined RprA binding to rpoS-L RNA at 37 °C, the K_d was ~300 nM and the addition of Hfq enhanced formation of the RprA·rpoS-L complex by 9-fold (data no shown). This improved agreement with the in vivo data lends supports to the relevance of the binding studies on the full leader region with respect to understanding the role of Hfq in RpoS regulation in vivo. We note that Hfq enhancement of the stability of the RprA·rpoS RNA complexes reflects enhanced association rates (Figure S2 of the Supporting Information). Both kinetic and thermodynamic perspectives may be needed to explain translation regulation of rpoS mRNA in vivo.

A comparison of our results for the interaction of Hfq with RprA with work on Hfq and DsrA reveals several common characteristics as well as differences. The similarities and differences may help identify what is important and what is not with regard to the interaction of Hfq with these sRNAs and their common *rpoS* target. For example, gel shift characteristics of Hfq binding to RprA and DsrA are quite similar in spite of the difference in RNA sequences and predicted secondary structures. Two gel complexes are observed for both sRNAs; the Hill cooperativity parameter of Hfq binding to RprA and DsrA was similar, and the saturation point of Hfq with respect to sRNA at high concentrations implies a 2:1 stoichiometry for both strong Hfq·sRNA complexes [Figure S1 of the Supporting Information (*27*)].

K_d values evaluated for the Hfq−RprA complexes, 24 and 96 nM, are the same as the values determined by Mikulecky et al. (*28*) for the Hfq−DsrA complexes observed in a gel shift assay. The affinity determined by Lease and Woodson (*27*) for the strong Hfq−DsrA complex (37 nM) is comparable to that of the corresponding Hfq−RrpA complex; however, the K_d for the second Hfq DsrA complex (667 nM) indicates a significantly lower affinity. The presence of nonspecific tRNA in the reactions of the latter study may account for the higher K_d value.

We note that Hfq binding to DsrA by isothermal titration calorimetry indicates a 1:1 Hfq_6·DsrA stoichiometry (*28*). This difference from the gel results may reflect a number of factors, including technical complications inherent in either approach. The change in solvent conditions that occurs during the onset of electrophoresis before macromolecules enter the gel may alter the distribution of Hfq bound to the RNA. Higher concentrations needed for calorimetry may promote DsrA dimers. While determining the stoichiometry under different conditions is important, the experiments indicate that under similar conditions Hfq forms complexes with stability and characteristics similar to those of these two sRNAs.

The comparison described above emphasizes similarities in Hfq binding to DsrA and RprA. We note two significant differences. First, the two sRNAs have different affinities for the full *rpoS* RNA leader region. The affinity of RprA for rpoS-L RNA (~2500 nM) is weaker than binding of DsrA for this *rpoS* RNA target region (~750 nM). The most likely explanation is the number of complementary base pairs between RprA and DsrA for the *rpoS* target region. Optimum alignment of RprA with the RBS region shows 11 of 13 consecutive nucleotides compared to 21 of 23 nucleotides for DsrA (*15*).

A second distinction between DsrA and RprA is how their binding to Hfq is influenced by amino acid mutations and the competition of $(A)_n$ sequences. Mutations to three residues on the distal surface of Hfq (Y25, I30, and K31) had little or no effect on the strong binding complex of Hfq with DsrA or to domain II of DsrA, but they drastically weaken binding to poly(A) sequences (*28, 36*). This together with the observation that poly(A) does not displace DsrA from Hfq (*30*) implies that Hfq binds DsrA primarily with its proximal surface. In contrast, poly(A) or A_{18} displaced RprA from Hfq (Figure 9A). A mutation on the distal as well as proximal surface weakened binding of Hfq to RprA. These results are puzzling since they appear to be inconsistent with the similar gel binding characteristics of Hfq for these sRNAs. Reconciling these observations will require additional structural information about the two complexes.

ACKNOWLEDGMENT

We are grateful to Adam Leon, Lively Lie, Sean Murray, and Sarah Paglioni for assisting in plasmid construction and protein purification. We acknowledge a reviewer for suggesting a side-by-side comparison of RprA with DsrA and the timely response.

SUPPORTING INFORMATION AVAILABLE

Binding of Hfq to RprA at 100 nM (Figure S1), effect of Hfq on the rates of formation of RprA·RpoS-S and RprA·RpoS-L complexes (Figure S2), analysis of binding of mutant Hfq proteins to RprA (Figure S3), and analysis of binding of mutant Hfq proteins to RpoS-S (Figure S4), and effect of Hfq on DsrA binding to RpoS-S and RpoS-L (Figure S5). This material is available free of charge via the Internet at http://pubs.acs.org.

REFERENCES

1. Gottesman, S., Storz, G., Rosenow, C., Majdalani, N., Repoila, F., and Wassarman, K. M. (2001) Small RNA regulators of translation: Mechanisms of action and approaches for identifying new small RNAs. *Cold Spring Harbor Symp. Quant. Biol. 66*, 353–362.
2. Storz, G., Opdyke, J. A., and Zhang, A. (2004) Controlling mRNA stability and translation with small, noncoding RNAs. *Curr. Opin. Microbiol. 7*, 140–144.
3. Gottesman, S. (2004) The small RNA regulators of *Escherichia coli*: Roles and mechanisms. *Annu. Rev. Microbiol. 58*, 303–328.
4. Majdalani, N., Vanderpool, C. K., and Gottesman, S. (2005) Bacterial small RNA regulators. *Crit. Rev. Biochem. Mol. Biol. 40*, 93–113.
5. Wassarman, K. M., Repoila, F., Rosenow, C., Storz, G., and Gottesman, S. (2001) Identification of novel small RNAs using comparative genomics and microarrays. *Genes Dev. 15*, 1637–1651.
6. Moll, I., Leitsch, D., Steinhauser, T., and Blasi, U. (2003) RNA chaperone activity of the Sm-like Hfq protein. *EMBO Rep. 4*, 284–289.
7. Franze de Fernandez, M. T., Eoyang, L., and August, J. T. (1968) Factor fraction required for the synthesis of bacteriophage Qβ-RNA. *Nature 219*, 588–590.
8. Tsui, H. C., Leung, H. C., and Winkler, M. E. (1994) Characterization of broadly pleiotropic phenotypes caused by an hfq insertion mutation in *Escherichia coli* K-12. *Mol. Microbiol. 13*, 35–49.
9. Sun, X., Zhulin, I., and Wartell, R. M. (2002) Predicted structure and phyletic distribution of the RNA-binding protein Hfq. *Nucleic Acids Res. 30*, 3662–3671.
10. Zhang, A., Wassarman, K. M., Ortega, J., Steven, A. C., and Storz, G. (2002) The Sm-like Hfq protein increases OxyS RNA interaction with target mRNAs. *Mol. Cell 9*, 11–22.
11. Moller, T., Franch, T., Hojrup, P., Keene, D. R., Bachinger, H. P., Brennan, R. G., and Valentin-Hansen, P. (2002) Hfq: A bacterial Sm-like protein that mediates RNA-RNA interaction. *Mol. Cell 9*, 23–30.
12. Arluison, V., Derreumaux, P., Allemand, F., Folichon, M., Hajnsdorf, E., and Regnier, P. (2002) Structural Modelling of the Sm-like Protein Hfq from *Escherichia coli*. *J. Mol. Biol. 320*, 705–712.
13. Sledjeski, D. D., Whitman, C., and Zhang, A. (2001) Hfq is necessary for regulation by the untranslated RNA DsrA. *J. Bacteriol. 183*, 1997–2005.
14. Zhang, A., Altuvia, S., Tiwari, A., Argaman, L., Hengge-Aronis, R., and Storz, G. (1998) The OxyS regulatory RNA represses rpoS translation and binds the Hfq (HF-I) protein. *EMBO J. 17*, 6061–6068.
15. Majdalani, N., Hernandez, D., and Gottesman, S. (2002) Regulation and mode of action of the second small RNA activator of RpoS translation, RprA. *Mol. Microbiol. 46*, 813–826.
16. Moller, T., Franch, T., Udesen, C., Gerdes, K., and Valentin-Hansen, P. (2002) Spot 42 RNA mediates discoordinate expression of the *E. coli* galactose operon. *Genes Dev. 16*, 1696–1706.
17. Geissmann, T. A., and Touati, D. (2004) Hfq, a new chaperoning role: Binding to messenger RNA determines access for small RNA regulator. *EMBO J. 23*, 396–405.
18. Kawamoto, H., Koide, Y., Morita, T., and Aiba, H. (2006) Base-pairing requirement for RNA silencing by a bacterial small RNA and acceleration of duplex formation by Hfq. *Mol. Microbiol. 61*, 1013–1022.
19. Antal, M., Bordeau, V., Douchin, V., and Felden, B. (2005) A small bacterial RNA regulates a putative ABC transporter. *J. Biol. Chem. 280*, 7901–7908.
20. Bossi, L., and Figueroa-Bossi, N. (2007) A small RNA downregulates LamB maltoporin in *Salmonella*. *Mol. Microbiol. 65*, 799–810.
21. Lenz, D. H., Mok, K. C., Lilley, B. N., Kulkarni, R. V., Wingreen, N. S., and Bassler, B. L. (2004) The small RNA chaperone Hfq and multiple small RNAs control quorum sensing in *Vibrio harveyi* and *Vibrio cholerae*. *Cell 118*, 69–82.
22. Altuvia, S., Weinstein-Fischer, D., Zhang, A., Postow, L., and Storz, G. (1997) A small, stable RNA induced by oxidative stress: Role as a pleiotropic regulator and antimutator. *Cell 90*, 43–53.
23. Brown, L., and Elliott, T. (1996) Efficient translation of the RpoS sigma factor in *Salmonella typhimurium* requires host factor I, an RNA-binding protein encoded by the hfq gene. *J. Bacteriol. 178*, 3763–3770.
24. Sledjeski, D. D., Gupta, A., and Gottesman, S. (1996) The small RNA, DsrA, is essential for the low temperature expression of RpoS during exponential growth in *Escherichia coli*. *EMBO J. 15*, 3993–4000.
25. Cunning, C., Brown, L., and Elliott, T. (1998) Promoter substitution and deletion analysis of upstream region required for rpoS translational regulation. *J. Bacteriol. 180*, 4564–4570.
26. Majdalani, N., Cunning, C., Sledjeski, D., Elliott, T., and Gottesman, S. (1998) DsrA RNA regulates translation of RpoS message by an anti-antisense mechanism, independent of its action as an antisilencer of transcription. *Proc. Natl. Acad. Sci. U.S.A. 95*, 12462–12467.
27. Lease, R. A., and Woodson, S. A. (2004) Cycling of the Sm-like protein Hfq on the DsrA small regulatory RNA. *J. Mol. Biol. 344*, 1211–1223.
28. Mikulecky, P. J., Kaw, M. K., Brescia, C. C., Takach, J. J., Sledjeski, D., and Feig, A. L. (2004) *Escherichia coli* Hfq has distinct interaction surfaces for DsrA, rpoS and poly(A) RNAs. *Nat. Struct. Mol. Biol. 11*, 1206–1214.
29. Afonyushkin, T., Vecerek, B., Moll, I., Blasi, U., and Kaberdin, V. R. (2005) Both RNase E and RNase III control the stability of sodB mRNA upon translational inhibition by the small regulatory RNA RyhB. *Nucleic Acids Res. 33*, 1678–1689.
30. Brescia, C. C., Mikulecky, P. J., Feig, A. L., and Sledjeski, D. D. (2003) Identification of the Hfq-binding site on DsrA RNA: Hfq binds without altering DsrA secondary structure. *RNA 9*, 33–43.
31. Udekwu, K. I., Darfeuille, F., Vogel, J., Reimegard, J., Holmqvist, E., and Wagner, E. G. (2005) Hfq-dependent regulation of OmpA synthesis is mediated by an antisense RNA. *Genes Dev. 19*, 2355–2366.
32. Vecerek, B., Rajkowitsch, L., Sonnleitner, E., Schroeder, R., and Blasi, U. (2008) The C-terminal domain of *Escherichia coli* Hfq is required for regulation. *Nucleic Acids Res. 36*, 133–143.
33. Schumacher, M. A., Pearson, R. F., Moller, T., Valentin-Hansen, P., and Brennan, R. G. (2002) Structures of the pleiotropic translational regulator Hfq and an Hfq-RNA complex: A bacterial Sm-like protein. *EMBO J. 21*, 3546–3556.
34. Sauter, C., Basquin, J., and Suck, D. (2003) Sm-like proteins in Eubacteria: The crystal structure of the Hfq protein from *Escherichia coli*. *Nucleic Acids Res. 31*, 4091–4098.
35. Nikulin, A., Stolboushkina, E., Perederina, A., Vassilieva, I., Blaesi, U., Moll, I., Kachalova, G., Yokoyama, S., Vassylyev, D., Garber, M., and Nikonov, S. (2005) Structure of *Pseudomonas aeruginosa* Hfq protein. *Acta Crystallogr. D61*, 141–146.
36. Sun, X., and Wartell, R. M. (2006) *Escherichia coli* Hfq binds A18 and DsrA domain II with similar 2:1 Hfq6/RNA stoichiometry using different surface sites. *Biochemistry 45*, 4875–4887.
37. Lange, R., Fischer, D., and Hengge-Aronis, R. (1995) Identification of transcriptional start sites and the role of ppGpp in the expression of rpoS, the structural gene for the sigma S subunit of RNA polymerase in *Escherichia coli*. *J. Bacteriol. 177*, 4676–4680.

38. Mathews, D. H., Disney, M. D., Childs, J. L., Schroeder, S. J., Zuker, M., and Turner, D. H. (2004) Incorporating chemical modification constraints into a dynamic programming algorithm for prediction of RNA secondary structure. *Proc. Natl. Acad. Sci. U.S.A. 101*, 7287–7292.

39. Fried, M. G., and Crothers, D. M. (1984) Equilibrium studies of the cyclic AMP receptor protein-DNA interaction. *J. Mol. Biol. 172*, 241–262.

40. Mohanty, B. K., Maples, V. F., and Kushner, S. R. (2004) The Sm-like protein Hfq regulates polyadenylation dependent mRNA decay in *Escherichia coli*. *Mol. Microbiol. 54*, 905–920.

41. Arluison, V., Hohng, S., Roy, R., Pellegrini, O., Regnier, P., and Ha, T. (2007) Spectroscopic observation of RNA chaperone activities of Hfq in post-transcriptional regulation by a small non-coding RNA. *Nucleic Acids Res. 35*, 999–1006.

BI800479P